Available online at www.sciencedirect.com
ScienceDirect
Journal of Power Sources 163 (2006) 135–143
JOURNAL OF POWER SOURCES
www.elsevier.com/locate/jpowsour

Electrochemical and solid-state NMR studies on $LiCoO_2$ coated with Al_2O_3 derived from carboxylate-alumoxane

George T.K. Fey [a,*], H.M. Kao [b], P. Muralidharan [a], T.P. Kumar [a], Y.D. Cho [a]

[a] *Department of Chemical and Materials Engineering, National Central University, Chung-Li, Taiwan, ROC*
[b] *Department of Chemistry, National Central University, Chung-Li, Taiwan, ROC*

Received 24 October 2005; received in revised form 20 January 2006; accepted 24 January 2006
Available online 2 March 2006

Abstract

The surface of $LiCoO_2$ cathodes was coated with various wt.% of Al_2O_3 derived from methoxyethoxy acetate-alumoxane (MEA-alumoxane) by a mechano-thermal coating procedure, followed by calcination at 723 K in air for 10 h. The structure and morphology of the surface modified $LiCoO_2$ samples have been characterized with XRD, SEM, EDS, TEM, BET, XPS/ESCA and solid-state ^{27}Al magic angle spinning (MAS) NMR techniques. The Al_2O_3 coating forms a thin layer on the surface of the core material with an average thickness of 20 nm. The corresponding ^{27}Al MAS NMR spectrum basically exhibited the same characteristics as the spectrum for pristine Al_2O_3 derived from MEA-alumoxane, indicating that the local environment of aluminum atoms was not significantly changed at coating levels below 1 wt.%. This provides direct evidence that Al_2O_3 was on the surface of the core materials. The $LiCoO_2$ coated with 1 wt.% Al_2O_3 sustained continuous cycle stability 13 times longer than pristine $LiCoO_2$. A comparison of the electrochemical impedance behavior of the pristine and coated materials revealed that the failure of pristine cathode performance is associated with an increase in the particle–particle resistance upon continuous cycling. Coating improved the cathode performance by suppressing the characteristic structural phase transitions (hexagonal to monoclinic to hexagonal) that occur in pristine $LiCoO_2$ during the charge–discharge processes.

Keywords: Al_2O_3 coated $LiCoO_2$; ^{27}Al MAS NMR; Lithium-ion battery; MEA-alumoxane

1. Introduction

$LiCoO_2$ has become an established positive electrode material for lithium-ion batteries because of its ease of production, cycle stability, high volumetric energy density, good power rates, high specific capacity, and high operating cell voltage. However, the complete delithiation of $LiCoO_2$ leads to thermodynamically unstable CoO_2, so for practical secondary battery applications, only around 0.5 Li ions per molecule are delithiated during the cycle, which translates to a charge capacity of 140 mA h g^{-1} compared to its theoretical capacity 274 mA h g^{-1} [1–3]. The volume changes are ascribed to crystallographic phase transitions that occurred in $LiCoO_2$ during the charge–discharge process at $x < 0.5$ in Li_xCoO_2 [1,4]. It is assumed that the structural degradation of the cathode is because of Co^{4+} ion diffusion and dissolution into the electrolyte due to HF and a disproportionate reaction that occurs at the surface [3]. Battery performance is strongly dependent on surface chemistry [3,5,6].

Many researchers have made considerable efforts to improve the electrochemical performance and cycle stability by doping and surface coating the cathode material. Several studies established that coating the surface with electrochemically inactive metal oxide significantly improves cycling stability and cell performance. The improved cycling performance and capacity retention of the high fracture-tough coated cathode is assumed to result from the shielding of 3d metal ion diffusion and dissolution into the electrolyte and the suppression of cycle-limiting phase transitions during the (de) intercalation processes [7]. Both layered and spinel oxides were extensively studied for their improvement in cycling stability by the surface coating technique. Al_2O_3 [7–11], MgO [6,12], TiO_2, ZrO_2 [9,11] and SiO_2 [13] coated to the core material enhanced the cycling behavior of the $LiCoO_2$ cathode.

* Corresponding author. Tel.: +886 3 425 7325; fax: +886 3 425 7325.
E-mail address: gfey@cc.ncu.edu.tw (G.T.K. Fey).

0378-7753/$ – see front matter © 2006 Elsevier B.V. All rights reserved.
doi:10.1016/j.jpowsour.2006.01.076

The precursor materials [9,11–17] used in the coating process play a vital role in structuring a uniform and well-adhered coating on the surface of the core material with low-temperature syntheses. Al_2O_3 as a coating material to improve the cycle stability of $LiCoO_2$ has been investigated by several groups [4,7–11,14]. However, Al_2O_3 coatings derived from precursors of carboxylate-alumoxanes possess better cycle stability than coatings from other precursor materials [15,17] and use environmentally benign chemicals. Carboxylate-alumoxanes, $[Al(O)_x(OH)_y(O_2CR)_z]_n$, consist of an alumina core surrounded by covalently bonded carboxylate ligands.

$LiCoO_2$ has isostructural layers with perfectly ordered hexagonal α-$NaFeO_2$ type structure with $R\bar{3}m$ space group having an ABCABC oxygen stacking [18]. The cobalt and lithium ions are located on alternate octahedral sites of the (1 1 1) plane. In our prior work [15,17] on Al_2O_3 coatings derived from alumoxanes, we suggested that the coating material exists as a thin layer and possibly formed a solid-solution of $LiAl_xCo_{1-x}O_2$. This suggestion was derived from the lattice parameters and previous literature [6,7]. However, according to the literature [19,20], Al-doped $LiCoO_2$ forms a $LiAl_xCo_{1-x}O_2$ solid-state solution in which possible Al coordination occupies the tetrahedral site instead of octahedral to substitute for Co in the range $x = 0.1$–0.3. The presence of Al in the tetrahedral positions results in a decrease in lithium ion diffusivity and, consequently, the $LiAl_xCo_{1-x}O_2$ cathode material displayed poor reversibility, whereas Al_2O_3-coated $LiCoO_2$ was found to possess improved cycling stability and the coating material remained on the surface, as shown through solid-state NMR studies [20]. This conclusion led us to focus again on studying whether the coating Al_2O_3 had formed as a solid-solution of $LiAl_xCo_{1-x}O_2$ or remained on the surface of the core materials during heat-treatment.

Solid-state ^{27}Al MAS NMR has been established as an efficient means of determining the coordination and local structure of specific aluminum species in aluminum oxides, since both tetrahedral and octahedral ^{27}Al sites can be readily resolved based on their distinctly different chemical shifts. Thus, the position of ^{27}Al resonance gives a good indication of the local environment of the aluminum site. For example, when the aluminum atoms are tetrahedrally coordinated to the framework, then a resonance in the range of 50–80 ppm is visible in the ^{27}Al NMR spectrum. The responding signal of octahedrally coordinated aluminum has a chemical shift at around 0 ppm [20]. Stewart et al. have shown that the ^{27}Al MAS NMR spectra provided more structural information than the ^{6}Li or ^{7}Li NMR spectra of $LiAl_5O_8$ [21]. Therefore, this paper presents the electrochemical studies of various wt.% of Al_2O_3 derived from MEA-alumoxane coated on the commercial $LiCoO_2$ by a mechano-thermal process. ^{27}Al MAS NMR was used to probe the change in the coordinations and local environments of aluminum species derived from MEA-alumoxane coated $LiCoO_2$.

2. Experimental

According to a procedure described by Callender et al. [22], MEA-alumoxane was synthesized from pseudo-boehmite, $[Al(O)(OH)]_n$ (Plural SB, average particle size: 45 μm; BET surface area: 250 $m^2\,g^{-1}$), and methoxyethoxy acetic acid, $[CH_3OCH_2CH_2OCH_2COOH]$ (Aldrich). The calculated wt.% of MEA-alumoxane was dispersed in double distilled water for 10 h and sonicated for 30 min with a commercial $LiCoO_2$ powder (average particle size: 1–8 μm, Coremax Taiwan Corporation) and stirred for 10 h at room temperature. Subsequently the mixture was heated at 323 K to eliminate most of the water by slow evaporation and obtain a thick slurry that was further dried in an oven at 383 K for 24 h. The result was a black dry mass of MEA-alumoxane coated $LiCoO_2$ particles. The obtained powder was calcined at 723 K in air for 10 h, when MEA-alumoxane decomposed to yield an adherent coating of γ-Al_2O_3 on the $LiCoO_2$ particles [23]. The weight ratios of $LiCoO_2$ to Al_2O_3, formed upon calcination, were 99.9:0.1, 99.7:0.3, 99.0:1.0, and 97.0:3.0. In addition, $LiCoO_2$ to Al_2O_3 samples were prepared in near weight ratios (99.5:0.5, 99.0:1.0, 98.5:1.5, 98.0:2.0, 97.5:2.5, 97.0:3.0 and 0:100) for ^{27}Al MAS NMR studies following the above procedure.

An X-ray diffractometer (XRD), Siemens D-5000, Mac Science MXP18, equipped with a nickel-filtered Cu Kα radiation source ($\lambda = 1.5405$ Å) was used for structural analysis. The diffraction patterns were recorded between scattering angles of 5° and 80° in steps of 0.05°. The Brunauer–Emmett–Teller (BET) surface area measurements were carried out on a Micromeritics ASAP 2010 surface area analyzer. The surface morphology of the coated materials was studied using a scanning electron microscope (SEM), Hitachi model S-3500V. The microstructures of the coated particles were examined by a JEOL JEM-200FXII transmission electron microscope (TEM) equipped with a LaB_6 gun. The samples for TEM studies were prepared by dispersing the coated powders in ethanol, placing a drop of the clear solution on a carbon-coated copper grid, and subsequent drying. X-ray photon spectroscopy (XPS) and the depth profiles of Aluminum, cobalt and oxygen were recorded by an electron spectroscopy for chemical analysis (ESCA) instrument (VG Scientific ESCALAB 250) with monochromatic Al Kα radiation 1486.6 eV. The survey spectra were scanned in the range 0.00–1000.00 eV binding energy (BE) in 0.50 eV steps.

^{27}Al MAS NMR spectra were recorded on a Bruker AVANCE-400 spectrometer, equipped with a 4 mm probe, with a resonance frequency of 104.26 MHz for ^{27}Al nucleus. All ^{27}Al MAS NMR spectra were obtained with a small flip angle of approximately 15° and with a recycle delay of 1 s. The ^{27}Al chemical shift was externally referenced to $Al(H_2O)_6^{3+}{}_{(aq)}$ at 0.0 ppm.

The cathodes for electrochemical studies were prepared by a doctor-blade coating method with a slurry of 85 wt.% coated active material, 10 wt.% conductive carbon black and 5 wt.% poly(vinylidene fluoride) as a binder, in *N*-methyl-2-pyrrolidone (NMP), as the solvent for the mixture, which was then applied onto an etched aluminum foil current collector and dried at 393 K for 12 h in an oven. The coated cathode foil was then smoothed by pressing it through stainless-steel twin rollers and then cut into circular discs 13 mm in diameter.

The electrochemical performance of the above discs were carried out with coin type cells of the 2032 configuration and were assembled in an argon-filled VAC MO40-1 glove

box in which the oxygen and water contents were maintained below 2 ppm. Lithium metal (Foote Mineral) was used as the anode and a 1 M $LiPF_6$ in ethylene carbonate:diethyl carbonate EC:DEC (1:1 v/v) (Tomiyama Chemicals) was used as the electrolyte with a Celgard membrane as the separator. The cells charge–discharge cycles were preformed at a 0.2 C rate between 2.75 and 4.40 V in a multi-channel battery tester (Maccor 4000).

Coin cells fully charged to 4.4 V were subjected to impedance measurements. The impedance spectra were recorded using a Schlumberger 1286 electrochemical interface and frequency response analyzer (Model 1255), driven by Corrware software (Scribner Associates). The frequency range was 65 kHz to 0.001 Hz and the amplitude of the perturbation signal was 20 mV. The impedance spectra were analyzed with Z-view software (Scribner Associates).

Phase transitions occurring during the cycling processes were examined by slow scan cyclic voltammetry, performed with a three-electrode glass cell. The working electrodes were prepared with the cathode powders as described above, but coated on both sides of the aluminum foil. The cells for the cyclic voltammetric studies were assembled inside the glove box with lithium metal foil serving as both counter and reference electrodes. The electrolyte used was the same as that for the coin cell. Cyclic voltammograms were run on a Solartron 1287 Electrochemical Interface at a scan rate of 0.1 m V s^{-1} between 3.0 and 4.4 V.

3. Results and discussion

3.1. X-ray diffraction

Fig. 1a shows the XRD pattern of the γ-Al_2O_3 obtained by the decomposition of MEA-alumoxane at 723 K [23]. A comparison with the JCPDS pattern in Fig. 1b confirms that the product was γ-Al_2O_3. Fig. 2a and b shows the XRD patterns of the γ-Al_2O_3 coated $LiCoO_2$ powder and pristine $LiCoO_2$, respectively. The diffraction patterns of all the materials conform to the $R\bar{3}m$ symmetry of the core material. The absence of diffraction patterns corresponding to Al_2O_3 may be due to a thin coating layer on the surface of the core material. In order to confirm the presence of Al_2O_3 as a coating layer formed on the surface of the core material, a ^{27}Al MAS NMR study was performed.

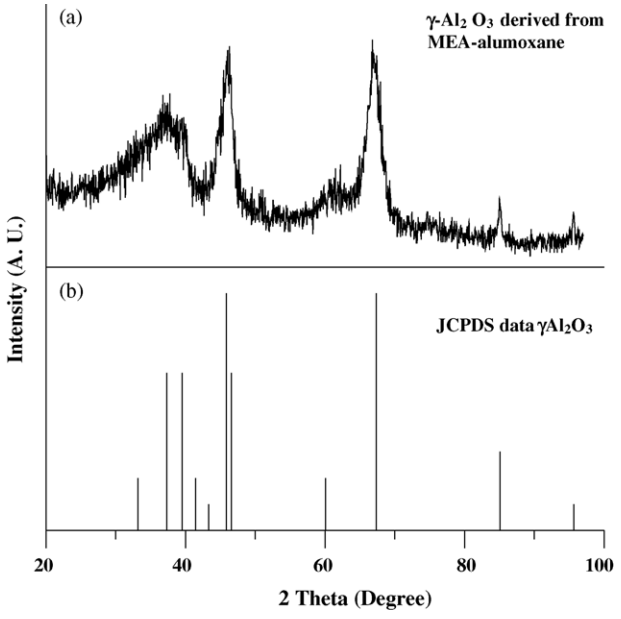

Fig. 1. Powder X-ray diffraction patterns of (a) Al_2O_3 derived from MEA-alumoxane by a mechano-thermal process and (b) JCPDS data γ-Al_2O_3.

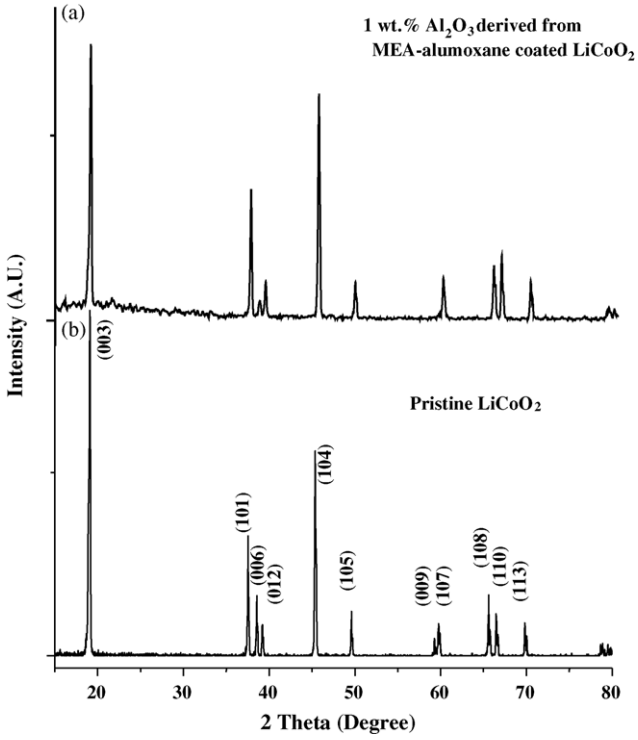

Fig. 2. Powder X-ray diffraction patterns of: (a) $LiCoO_2$ coated with 1 wt.% Al_2O_3 derived from MEA-alumoxane by a mechano-thermal process and (b) pristine $LiCoO_2$.

3.2. ^{27}Al MAS NMR

The ^{27}Al MAS NMR experiments were performed in order to obtain complementary information about the local environment of aluminum atoms. Fig. 3 shows the ^{27}Al MAS NMR spectra of Al_2O_3 derived from MEA-alumoxane on $LiCoO_2$ as a function of coating levels, together with that of the pristine Al_2O_3 derived from MEA-alumoxane for comparison. As shown in Fig. 3e, the ^{27}Al NMR spectrum of the pristine Al_2O_3 derived from MEA-alumoxane sample exhibited two resonance peaks centered at about 7 and 70 ppm for octahedral and tetrahedral of aluminum sites, respectively. The asymmetric line shape for the peak at 7 ppm with a tail to negative shift was resulted from the second-order quadrupolar effects, which are only partially averaged out by MAS. When a low concentration of about 1.0 wt.% of MEA-alumoxane was coated on $LiCoO_2$, the ^{27}Al MAS NMR spectrum was basically the same as for the pristine Al_2O_3 derived from MEA-alumoxane in Fig. 3d, except with a poor *S/N* ratio, indicating that the local environment of aluminum atoms had not changed significantly upon coating. This also provides

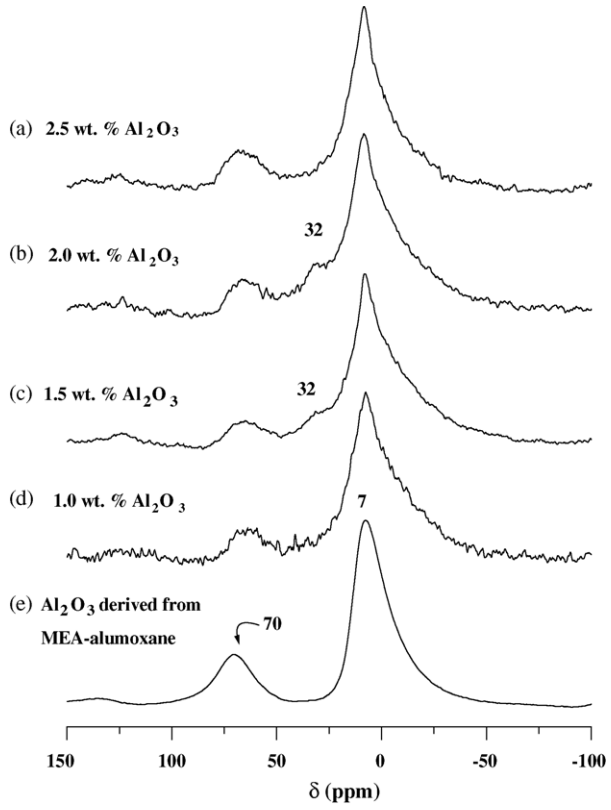

Fig. 3. ^{27}Al MAS NMR spectra of Al_2O_3 coated $LiCoO_2$ as a function of coating level: (a) 2.5 wt.%, (b) 2.0 wt.%, (c) 1.5 wt.%, (d) 1.0 wt.%, and (e) 0 wt.%.

direct evidence of the presence of Al_2O_3 derived from MEA-alumoxane on the surface of $LiCoO_2$. Since no large change in chemical shifts due to paramagnetic effects was observed, the aluminum species in MEA-alumoxane was far from, at least on an atomic level, the core $LiCoO_2$ materials. On the other hand, when the concentration of coated MEA-alumoxane reached 1.5–2.0 wt.%, a new shoulder at around 32 ppm was observed in Fig. 3b and c. However, this shoulder disappeared when the coating level was higher than 2.5 wt.%, as in Fig. 3a. The resonance peak at around 32 ppm was usually assigned to five-coordinated aluminum species or tetrahedral aluminum with a large quadrupolar coupling constant [19,21,24]. This observation suggests that a possible distortion of the crystal structure of Al_2O_3 derived MEA-alumoxane occurred at a coating level between 1.5 and 2.0 wt.%, which also correlates with the results of electrochemical properties of these materials at 3 wt.% coating levels.

Tirado et al. [19] have studied the cobalt effects on the ^{27}Al NMR chemical shifts in $LiAl_xCo_{1-x}O_2$ solid-solution. According to their studies, different Al environments, for example, Al(3Co$_3$Al) at 42 ppm, Al(2Co$_4$Al) at 35 ppm, and Al(1Co$_5$Al) at 28 ppm, which are closer to our observation of 32 ppm peak, have been assigned. Thus, the possibility of forming $LiAl_xCo_{1-x}O_2$ solid-solution during the coating process cannot be totally excluded. This is also well correlated with the results of electrochemical properties of these materials. The electrochemical properties were optimized at a coating level of 1.0 wt.%. However, this shoulder disappeared when the coating level was 2.5 wt.% and higher. It is also interesting to note that the line width of the resonance peak at around 7 ppm of all Al_2O_3 derived MEA-alumoxane coated $LiCoO_2$ materials studied was significantly wider than that of the pristine Al_2O_3 derived MEA-alumoxane, indicating that the octahedral aluminum species in the former exhibited a larger second-order quadrupolar interaction, which might result from a subtle distortion in the local environment of aluminum induced by the coating process. From the present ^{27}Al NMR work, it was concluded that a crucial change in the structure of Al_2O_3 derived from MEA-alumoxane occurred when the coating level was in the range of 1.5–2.0 wt.%, while only a subtle change in the local environment of octahedral aluminum was observed at other coating levels.

3.3. Morphology

Fig. 4a–c shows the SEM micrographs of the pristine $LiCoO_2$, 1 wt.% Al_2O_3 coated $LiCoO_2$ powder and the EDS graph of the 1 wt.% Al_2O_3 coated $LiCoO_2$ powder, respectively. From Fig. 4a and b, it was observed that the surface of the cathode particles is distinctly changed upon coating. The increase in brightness of the material observed for the coated sample compared to the pristine sample is associated with the accumulation of charge on the non-conducting coating material (Al_2O_3) as the electron beam impinges on it. Thus, it shows that the surface remained coated with enough Al_2O_3 to form a uniform coating on the cathode material. From Fig. 4c, it is observed that the EDS results revealed the presence of Al, Co and O elemental peaks clearly. The atomic wt.% and element wt.% of Al, Co and O were presented as an inset table in Fig. 4c, which confirmed the presence of the composition of coated Al_2O_3 on the surface of the $LiCoO_2$ cathode particles.

Fig. 5 shows the TEM micrograph of 1.0 wt.% Al_2O_3 coating derived from MEA-alumoxane on $LiCoO_2$. The alumina coating formed a uniform and compact kernel (translucent region) over the $LiCoO_2$ particle (dark opaque region) and the thickness of the kernel was around 20 nm. The BET surface areas of the pristine and the 1.0 wt.%, MEA-alumoxane coated powders were 0.62 and 1.30 $m^2\,g^{-1}$, respectively. The increased surface area of the cathode material may be due to the greater surface area of the alumina generated by the decomposition of the MEA-alumoxane.

3.4. XPS/ESCA

An XPS was used to study the surface composition of the Al_2O_3 derived from MEA-alumoxane coated $LiCoO_2$ and also determine whether the coating Al_2O_3 had formed a solid-solution (e.g., $LiAl_xCo_{1-x}O_2$) or remained on the surface of the core materials. Fig. 6a and b shows the XPS spectra of Al 2p and O 1s at surface etch levels of 0 and 10 nm, respectively, for the coated material. From Fig. 6a, the observed binding energy of the Al 2p is 74.0 eV, which is in good agreement with the reported data [25]. The well resolved peak of Al 2p, 74.0 eV was observed at an etch level of 0 and a very low intense peak could be observed at level 10 nm, which is evidence that Al

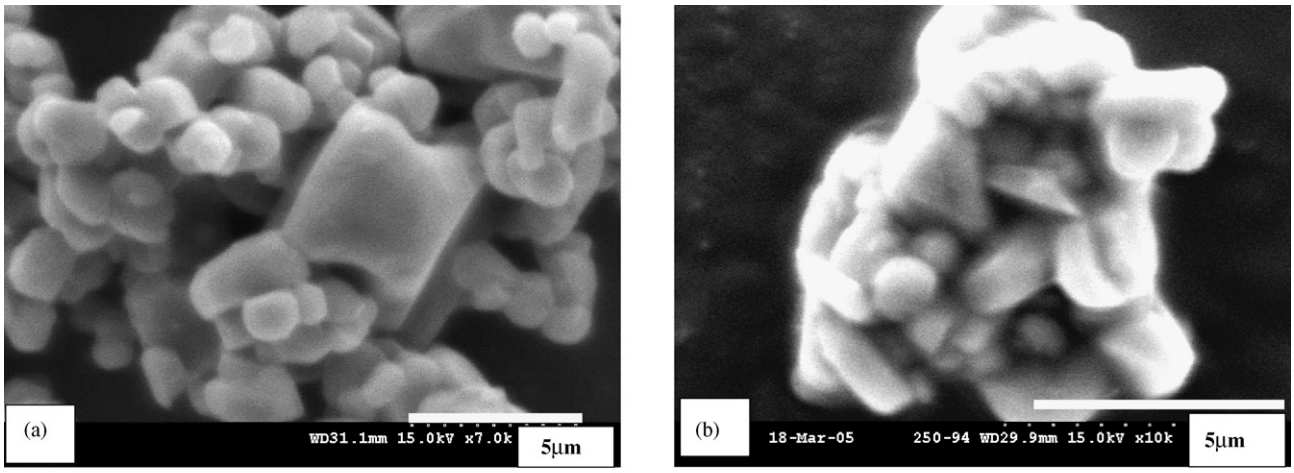

Pristine $LiCoO_2$

1 wt.% Al_2O_3 derived from MEA-alumoxane coated $LiCoO_2$

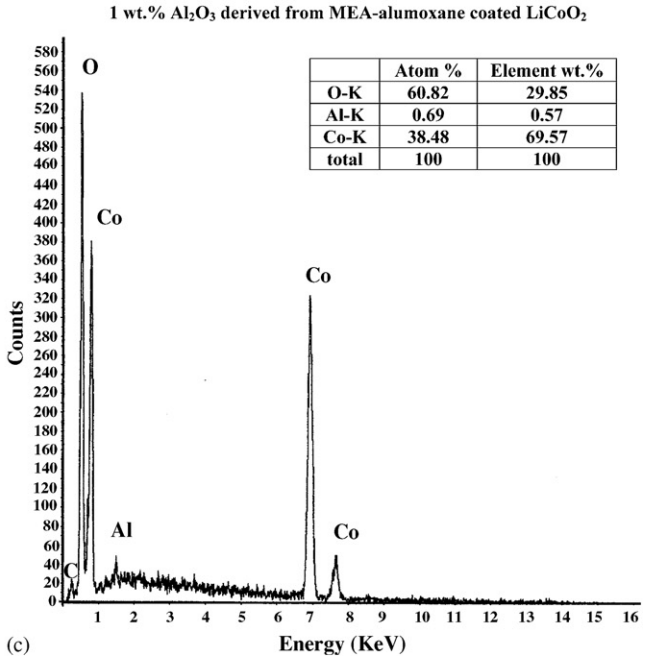

	Atom %	Element wt.%
O-K	60.82	29.85
Al-K	0.69	0.57
Co-K	38.48	69.57
total	100	100

Fig. 4. SEM images of: (a) pristine, (b) 1.0 wt.% Al_2O_3 coated $LiCoO_2$ particle, and (c) EDS graph of 1.0 wt.% Al_2O_3 coated $LiCoO_2$ particle by a mechano-thermal process.

is present at the surface of the core material. In Fig. 6b, an intense peak was observed at a binding energy of O 1s was 531.97 eV at an etch level of 0 with a shoulder at 531.97 eV and an intense peak at 529.75 eV binding energies at an etch level of 10 nm. The O 1 s binding energy of 531.97 eV corresponds to the Al_2O_3 and 529.75 eV refers to the pristine materials [25]. The 529.75 eV value does not change for several etching levels [25]. Thus, it could be concluded that Al_2O_3 coating has no influence on the chemical state or the binding energies of the different ions in the pristine material. This confirms that coated Al_2O_3 remained on the surface and there was no interaction with core material to form a solid-solution, as is evident from NMR results.

The inset in Fig. 7 shows the spatial distribution of the constituent elements concentration in the Al_2O_3 coated $LiCoO_2$ with the depth profile of the particle. Fig. 7 shows the Al atomic concentration with the depth profile and the inset figure shows the Co and oxygen concentration levels. The high atomic concentration of oxygen at the surface of the oxide is reasonable due to the presence of Al_2O_3 oxygen content. The concentration of cobalt increased to a depth of about 20 nm and then leveled off. The concentration of aluminum was low, typically less than the 2 at.% and there was an attendant decrease in the aluminum concentration with the depth of the particle. The depth profile value corresponds approximately to the thickness of the kernel observed with a TEM micrograph.

3.5. Electrochemical properties

3.5.1. Galvanostatic cycling

Fig. 8 shows the charge–discharge curves of the pristine $LiCoO_2$ and 0.1, 0.3, 1.0 and 3.0 wt.% of Al_2O_3 derived from MEA-alumoxane coated $LiCoO_2$. The first cycle capacities of those materials were 168, 167, 165, 168 and 144 mA h g^{-1}, respectively, for coating levels of 0.0, 0.1, 0.3, 1.0 and 3.0 wt.%. The generally lower capacities of the coated samples compared to the pristine sample are attributed to the presence of electroinactive alumina on the surface and/or to the lesser number of Co^{3+} ions available on the modified surface. Thus, the electrochemical studies reveal that the presence of the outer surface coating layer is formed of Al_2O_3. Cycling studies showed that a coating level of 1.0 wt.% yielded better cycle stability compared to the other wt.% coated samples. The charge–discharge curves in Fig. 8 show that the coating enhanced the cycle stability of the cathode material. We preset a cut-off value of 80% capacity retention, calculated with the first-cycle discharge capacity of the respective material, to compare with the number of cycles the cathode materials could sustain. Based on this cut-off regime, the pristine $LiCoO_2$ could sustain just 14 cycles. The numbers of cycles sustained by 0.1 and 0.3 wt.% Al_2O_3 coated materials were 58 and 65 cycles, respectively. When the coating level was increased to 1.0 wt.%, the cycle stability increased to 184 cycles which is 13 times more than the 14 cycles sustained by the pristine $LiCoO_2$ cathode.

In practice, a lower coating level of 0.1 or 0.3 wt.% was advantageous, but could not result in a sufficiently compact coating on the core material. However, when the coating level was increased further to 3.0 wt.%, the cycle stability and initial capacity declined drastically. The electrochemical results agree with the NMR results. It is clear that at a coating level of 3.0 wt.%, the coating material partially insulated the cathode particles, lowering the capacity utilization and cycle stability. The presence of excess coating material between the particles can also lower the particle–particle electronic conductivity and adversely affect the Coulombic efficiency.

The improved cycle stability of the cathode shows that the Al_2O_3 coating on the surface shielded the core material against HF attack at a high voltage of 4.4 V. It has also been reported [26] that ZrO_2 coated $LiMn_2O_4$ showed improved cycle stability, due to the negatively charged, amphoteric surface that

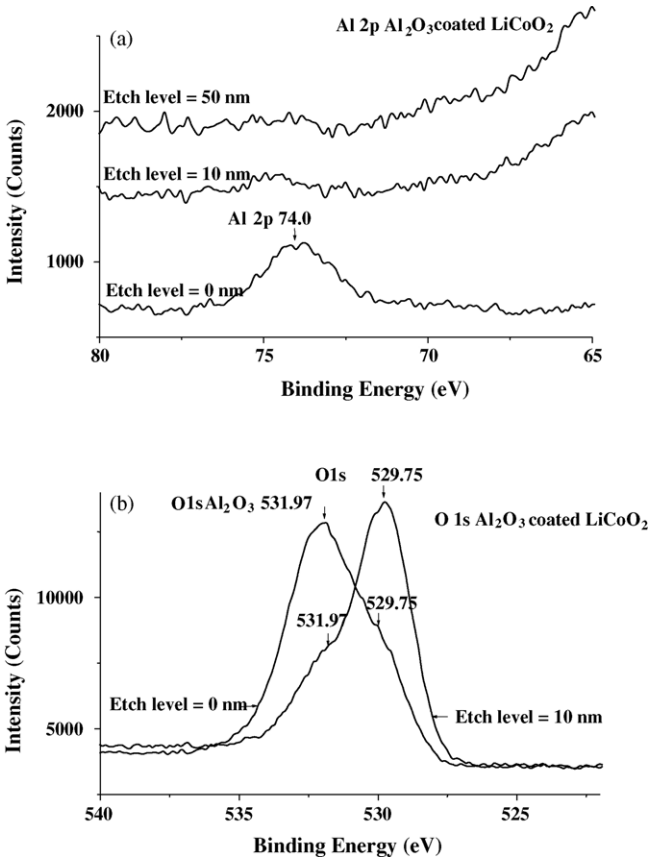

Fig. 6. XPS spectra: (a) Al 2p and (b) O 1 s of a 1 wt.% Al_2O_3 coated $LiCoO_2$ particle.

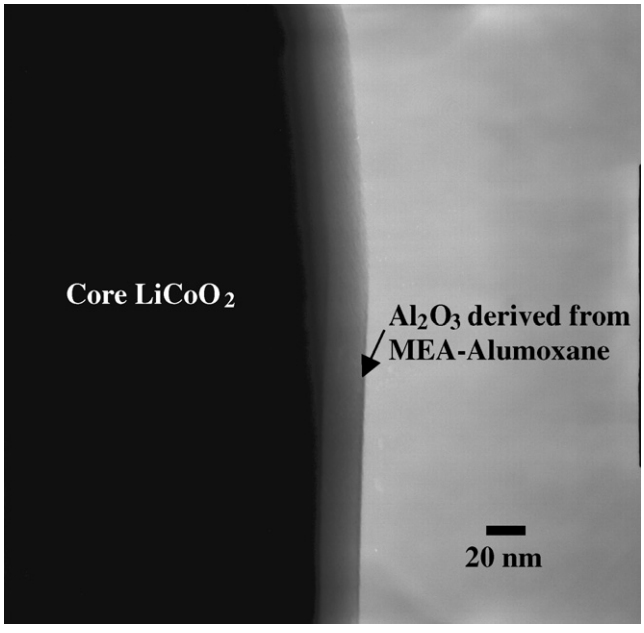

Fig. 5. TEM image of a 1.0 wt.% Al_2O_3 coated $LiCoO_2$ particle by a mechanothermal process.

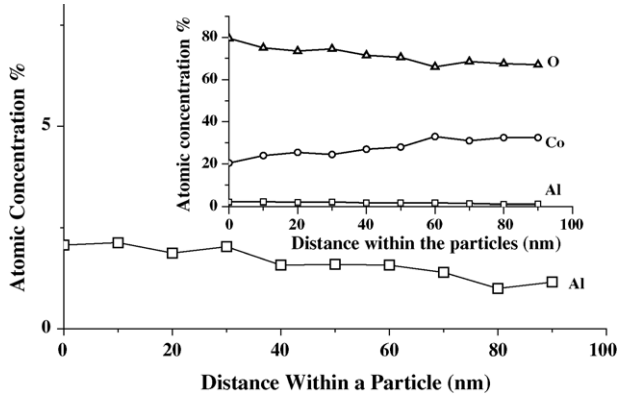

Fig. 7. Depth profile of a 1 wt.% Al_2O_3 coated $LiCoO_2$ particle. Inset: depth profiles of aluminum, cobalt and oxygen in a $LiCoO_2$ sample.

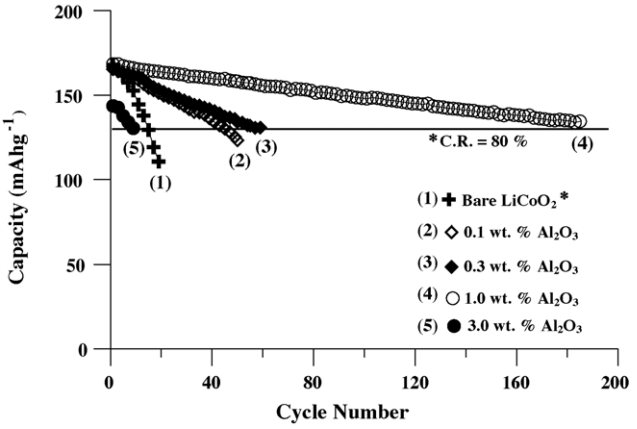

Fig. 8. Cycling performance of the pristine and alumina coated $LiCoO_2$ by the mechano-thermal process. Charge–discharge: 2.75∼4.40 V; 0.2 C rate.

scavenges the acidic HF species from the $LiPF_6$ liquid electrolyte. In the present study, since Al_2O_3 is also an amphoteric oxide, this explanation is relatively suitable for the Al_2O_3 coating on $LiCoO_2$. Thus, from XRD structural studies, TEM examination, XPS/ ESCA depth profile analysis and ^{27}Al MAS NMR results, we showed that the coated $LiCoO_2$ cathode particles were enveloped by a compact kernel consisting of an aluminum oxide formed by the decomposition of MEA-alumoxane on the core $LiCoO_2$ during the calcination step. Therefore, the coating is formed of Al_2O_3 on the outer surface of the core material and not as a solid-solution [15,17].

Apart from the improved cycle stability of the coated materials, a coating process based on MEA-alumoxane is more attractive for a number of reasons when compared to sol–gel precursor materials: (a) commercially available and lower cost mineral pseudo-boehmite alkoxy-substituted acetic acid, (b) the nanoparticulate precursor is infinitely stable in solid form, as well as in aqueous solution, and (c) the absence of environmentally hazardous vapors during processing, especially during calcination of green bodies of the coating material.

3.5.2. Electrochemical impedance

The electrical impedance spectroscopy (EIS) response of the $LiCoO_2$ cathode in a non-aqueous electrolyte reveals the processes such as the transport of lithium ions in the electrolyte, charge-transfer across the electrode–electrolyte interface, and adsorption of absorbed lithium ions into the solid oxide matrix [27,28]. Fig. 9a and b compares the EIS profiles of the pristine and Al_2O_3-coated $LiCoO_2$ samples at the charge potential of 4.4 V, respectively, as a function of cycle number. All the EIS profiles in Fig. 9a and b consist of a high-frequency semicircle that represents the impedance due to a solid-state interface layer formed on the surface of the electrodes, and a low-frequency semicircle that is related to a slow charge-transfer process at the interface and its relative double-layer capacitance at the film/bulk oxide. The Warburg impedance related to a combination of the diffusional effects of lithium ions on the interface between the active material particles and electrolyte, which is generally indicated by an inclined straight line at the low-frequency end. The impedance spectra were analyzed by Z-view

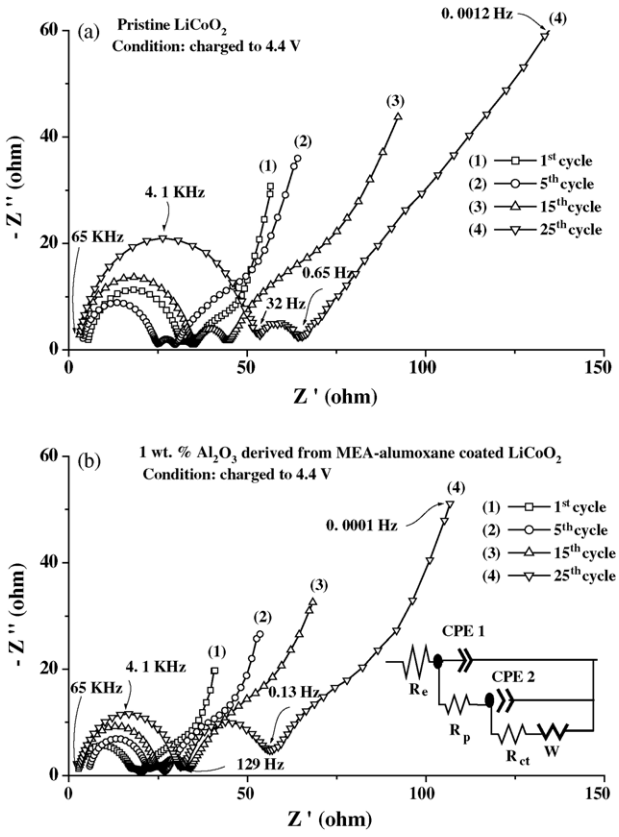

Fig. 9. Impedance spectra (Z′ vs. Z″) of (a) pristine and (b) 1 wt.% Al_2O_3 coated $LiCoO_2$ as a function of cycle number.

software and the data fitted to the equivalent circuit shown in the inset of Fig. 9b. Here, R_e is the electrolyte resistance, R_p the particle–particle resistance, R_{ct} the charge-transfer resistance, W the Warburg impedance, and CPE1 and CPE2 are constant phase elements.

As can be seen from Table 1, the solution resistance, R_e, undergoes very small changes upon cycling. The minor changes in solution resistance are attributed to the complicated chemistry

Table 1
Electrolyte, particle–particle, and charge-transfer resistances of pristine and 1 wt.% Al_2O_3 coated $LiCoO_2$

Cathode	Cycle number	R_e (Ω)	R_p (Ω)	R_{ct} (Ω)
Pristine $LiCoO_2$	1	5.56	15.74	5.14
	5	4.61	17.39	6.99
	10	2.41	22.46	7.50
	15	2.55	30.65	8.70
	20	2.63	40.85	14.40
	25	2.46	47.85	23.03
	30	3.25	75.52	30.41
1 wt.% Al_2O_3 coated $LiCoO_2$	1	2.59	1.44	4.92
	5	2.63	14.82	5.93
	10	2.28	18.32	7.39
	15	2.76	20.66	9.02
	20	2.55	24.32	18.50
	25	2.48	28.15	24.26
	30	2.69	32.25	34.02

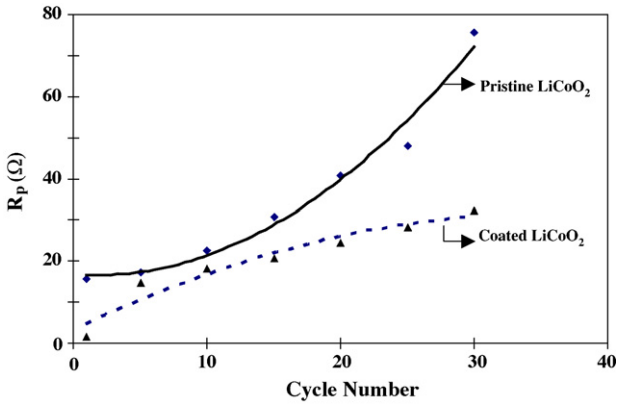

Fig. 10. Variation in the particle–particle resistance of pristine and Al_2O_3 coated $LiCoO_2$ as a function of cycle number.

of lithium in electrolyte solutions, which leads to slight changes in the content of the conducting species in the solution [29]. However, the size of the high-frequency semicircle increased with cycling in the case of the pristine cathode material. In Table 1, the charge-transfer resistance, R_{ct}, of the cathode materials increased with continuous cycling. However, the variations in R_{ct} with cycling for the two cathodes were comparable, which suggests that the intercalation characteristics of the cathode did not change after coating.

Table 1 compares the changes in particle–particle resistance, R_p, of the pristine and coated cathodes as a function of cycle number and Fig. 10 shows that the resistance of the surface film on the pristine cathode particles increased faster than the resistance of the film on the coated cathode. As a result, we conclude that pristine $LiCoO_2$ has a passive surface film of polycarbonates, polymeric hydrocarbons, Li_2CO_3, LiF, Li_xPF_y and $Li_xPF_yO_z$ [30–33] because of direct interaction of pristine $LiCoO_2$ with the harmful electrolyte, which makes it more prone to increases in the surface resistance of particles of the cathode material and thereby, hinders the diffusion of lithium ions during continuous cycling. The passive surface film formation was evident from Edstrom et al. [33] XPS analysis of the cathode material ($LiNi_{0.8}Co_{0.2}O_2$, $LiCoO_2$, $LiFePO_4$).

On the other hand, the slower increase in the particle–particle resistance value (Fig. 10) for the coated cathode suggests that the Al_2O_3 coating on its particles protects the active surface of the cathode material from direct interaction with the harmful electrolyte, which makes it less prone to changes in surface film composition during continuous cycling. As referred to the galvanostatic cycling section, Al_2O_3 is an amphoteric oxide and the negatively charged amphoteric surface acts as a scavenger on the acidic HF species from the $LiPF_6$ liquid electrolyte [26]. Therefore, the slower increase in the resistance of the surface film implies that the alumina coating resulted in a more stable cathode surface, which bestowed a longer cycle life to the cathode. Based on the studies of Aurbach et al. [34], when $LiCoO_2$ cathodes undergo a gradual degradation upon cycling, the major capacity fade mechanism involves the formation and thickening of surface films. The impedance spectroscopy proves that cathode materials coated with Al_2O_3 protect the surface from the electrolyte and thereby improve cell cycle stability and capacity retention.

3.5.3. Cyclic voltammetry

The electrochemical behavior and structural changes of $LiCoO_2$ in the potential region 4.4 V have been investigated through cyclic voltammetry study. $LiCoO_2$ is known to undergo a hexagonal–monoclinic–hexagonal phase transition above 4.1 V versus Li^+/Li that leads to capacity fade upon repeated cycling [1–3]. According to Kavan and Gratzel [35], cyclic voltammetry is sensitive to phase transformations occurring during electrochemical reactions. Thus, slow scan cyclic voltammetry was performed in order to examine the effect of the coating on the phase transitions that accompany the charge–discharge processes and the same is reported elsewhere [15,17]. The CV of pristine $LiCoO_2$ and 1.0 wt.% Al_2O_3 coated $LiCoO_2$ showed phase transitions from the hexagonal to monoclinic to hexagonal during the first cycle. The peaks were found to be distinctly suppressed from the second cycle onwards, which indicates that there is no transition from hexagonal to monoclinic phase, the major cause for structural degradation in $LiCoO_2$. Therefore, it is clear that the absence of phase transition means that insignificant strain and micro cracks that may be present initially are repaired electrochemically upon cycling. Thus, as the lattice contracts and expands during the cycling processes, the surface texture of the active material particles changes, enabling the coating material to become adhered in the fracture on the cathode surface. According to Cho et al. [7], a fracture-tough oxide kernel over $LiCoO_2$ can suppress volume changes accompanying the cycling processes. The more compact kernel that results leads to the suppression of phase transitions, cycle stability enhancement of the coated material, and longer cycle life.

4. Conclusions

Commercial $LiCoO_2$ cathode materials were coated effectively with various wt.% Al_2O_3 derived from MEA-alumoxane by a mechano-thermal method. The XRD patterns of the coated materials did not show any extraneous peaks corresponding to the Al_2O_3 coated particles. The TEM images of 1.0 wt.% Al_2O_3 coated particles revealed that the oxide formed a compact coating over the cathode particles. The solid-state ^{27}Al NMR results confirmed that coated Al_2O_3 remained on the surface of the core material and did not react with it to form a solid-solution that could modify the crystal structure and the electrochemical properties of the material. A crucial change in the crystal structure of MEA-alumoxane was observed in the ^{27}Al NMR spectrum when the coating level was higher than 1.0 wt.% as it is the optimum coating concentration. In addition, XPS results confirmed the coated Al_2O_3 remained on the surface of the core material. Galvanostatic cycling studies showed an enhancement in the cycle stability of $LiCoO_2$ was achieved by a 1.0 wt.% Al_2O_3 coating whose cycling stability is 13 times better than the 14 cycles sustained by the pristine cathode. Impedance spectra of the coated cathode suggest that the Al_2O_3 surface coating on $LiCoO_2$ reduces changes in the surface film during

electrochemical cycling, resulting in a longer cycle life. The results are complemented by slow scan cyclic voltammetric profiles, which show that the alumina coatings led to a suppression of the cycle-limiting phase transitions.

Acknowledgements

Financial support for this work was provided by the National Science Council of the Republic of China under contract No. NSC 93-2214-E-008-004. PMD thanks the NSC for the award of a post-doctoral fellowship.

References

[1] H.F. Wang, Y.I. Jang, B.Y. Huang, D.R. Sadoway, Y.M. Chiang, J. Electrochem. Soc. 146 (1999) 473.
[2] E. Plichita, S. Slane, M. Uchiyama, M. Salomon, D. Chua, W.B. Ebner, H.W. Lin, J. Electrochem. Soc. 136 (1989) 1865.
[3] G.G. Amatucci, J.M. Tarascon, L.C. Klein, Solid State Ionics 83 (1996) 167.
[4] S. Lavasseur, M. Menetrier, E. Suard, C. Delmas, Solid State Ionics 128 (2000) 11.
[5] D. Aurbach, K. Gamosky, B. Markovsky, G. Salitra, Y. Gofer, U. Heider, R. Oesten, M. Schmidt, J. Electrochem. Soc. 147 (2000) 1322.
[6] Z. Wang, C. Wu, L. Liu, F. Wu, F. Wu, L. Chen, X. Huang, J. Electrochem. Soc. 149 (2002) A466.
[7] J. Cho, Y.J. Kim, B. Park, Chem. Mater. 12 (2000) 3788.
[8] J. Cho, Y.J. Kim, B. Park, J. Electrochem. Soc. 148 (2001) A1110.
[9] J. Cho, Y.J. Kim, T.-J. Kim, B. Park, Angew. Chem. Int. Ed. 40 (2001) 3367.
[10] L. Liu, Z. Wang, H. Li, L. Chen, X. Huang, Solid State Ionics 152/153 (2002) 341.
[11] A.M. Kannan, L. Rabenberg, A. Manthiram, Electrochem. Solid State Lett. 6 (2003) A16.
[12] M. Mladenov, R. Stoyanova, E. Zhecheva, S. Vassilev, Electrochem. Commun. 3 (2001) 410.
[13] G.T.K. Fey, H.Z. Yang, T.P. Kumar, S.P. Naik, A.S.T. Chiang, D.C. Lee, J.R. Lin, J. Power Sources 132 (2004) 172.
[14] G.T.K. Fey, Z.X. Weng, J.G. Chen, C.Z. Lu, T.P. Kumar, S.P. Naik, A.S.T. Chiang, D.C. Lee, J.R. Lin, J. Appl. Electrochem. 34 (2004) 715.
[15] G.T.K. Fey, J.G. Chen, T.P. Kumar, J. Appl. Electrochem. 35 (2005) 177.
[16] G.T.K. Fey, C.Z. Lu, T.P. Kumar, Y.C. Chang, Surf. Coat. Technol. 199 (2005) 22.
[17] G.T.K. Fey, J.G. Chen, T.P. Kumar, J. Power Sources 146 (2005) 250.
[18] H.J. Orman, P.J. Wiseman, Acta Crystallogr. C (1984) 12.
[19] R. Alcántara, P. Lavela, P.L. Relaño, J.L. Tirado, Inorg. Chem. 37 (1998) 264.
[20] Y. Lee, A. Woo, K.-S. Han, K.S. Ryu, D. Sohn, D. Kim, H. Lee, Electrochim. Acta 50 (2004) 489.
[21] F.F. Stewart, J.F. Stebbins, E.S. Peterson, Y. Farnan, S.O. Dunham, E. Adams, P.W. Jennings, Chem. Mater. 7 (1995) 363.
[22] R.L. Callender, C.J. Harlan, N.M. Shapiro, C.D. Jones, D.L. Callahan, M.R. Wiesner, D.B. MacQueen, R. Cook, A.R. Barron, Chem. Mater. 9 (1997) 2418.
[23] R.L. Callender, A.R. Barron, Adv. Mater. 12 (2000) 734.
[24] K.J.D. MacKenzie, M.E. Smith, Multinuclear Solid-State NMR of Inorganic Materials, Pergamon, 2002, p. 283.
[25] http://www.xpsdata.com/XI_BE_Lookup_table.pdf.
[26] M.M. Thackeray, C.S. Johnson, J.-S. Kim, K.C. Lauzze, J.T. Vaughey, N. Dietz, D. Abraham, S.A. Hackney, W. Zeltner, M.A. Anderson, Electrochem. Commun. 5 (2003) 752.
[27] F. Croce, F. Nobili, A. Deptula, W. Lada, R. Tossici, A. D'Epifanio, B. Scrosati, R. Marassi, Electrochem. Commun. 1 (1999) 605.
[28] F. Nobili, F. Croce, B. Scrosati, R. Marassi, Chem. Mater. 13 (2001) 1642.
[29] D. Aurbach, A. Schechter, Electrochim. Acta 46 (2001) 2395.
[30] D. Aurbach, M.D. Levi, E. Levi, H. Teller, B. Markovsky, G. Salitra, L. Heider, U. Heider, J. Electrochem. Soc. 145 (1998) 3024.
[31] D. Aurbach, B. Markovsky, M.D. Levi, E. Levi, A. Schechter, M. Moshkovich, Y.S. Cohen, J. Power Sources 81/82 (1999) 95.
[32] D. Aurbach, B. Markovsky, A. Rodkin, E. Levi, Y.S. Cohen, H.J. Kim, M. Schmidt, Electrochim. Acta 47 (2002) 4291.
[33] K. Edstrom, T. Gustafsson, J.O. Thomas, Electrochim. Acta 50 (2004) 395.
[34] D. Aurbach, B. Markovsky, A. Rodkin, M. Cojocaru, E. Levi, H.J. Kim, Electrochim. Acta 47 (2002) 1899.
[35] L. Kavan, M. Gratzel, Electrochem. Solid-State Lett. 5 (2002) A39.